Flat-Band-Enabled Triplet Excitonic Insulator in a Diatomic Kagome Lattice

Gurjyot Sethi,[1] Yinong Zhou,[1] Linghan Zhu,[2] Li Yang,[2,3] and Feng Liu[1]
[1]Department of Materials Science and Engineering, University of Utah, Salt Lake City, Utah 84112, USA
[2]Department of Physics, Washington University in St. Louis, St. Louis, Missouri 63130, USA
[3]Institute of Materials Science and Engineering, Washington University in St. Louis, St. Louis, Missouri 63130, USA

(Received 21 November 2020; accepted 15 April 2021; published 12 May 2021)

The excitonic insulator (EI) state is a strongly correlated many-body ground state, arising from an instability in the band structure toward exciton formation. We show that the flat valence and conduction bands of a semiconducting diatomic Kagome lattice, as exemplified in a superatomic graphene lattice, can possibly conspire to enable an interesting triplet EI state, based on density-functional theory calculations combined with many-body *GW* and Bethe-Salpeter equation. Our results indicate that massive carriers in flat bands with highly localized electron and hole wave functions significantly reduce the screening and enhance the exchange interaction, leading to an unusually large triplet exciton binding energy (∼1.1 eV) exceeding the *GW* band gap by ∼0.2 eV and a large singlet-triplet splitting of ∼0.4 eV. Our findings enrich once again the intriguing physics of flat bands and extend the scope of EI materials.

DOI: 10.1103/PhysRevLett.126.196403

The discovery of the excitonic insulator (EI) state has been a sought-after endeavor since it was first proposed by Kohn [1,2] about fifty years ago. The EI phase is an exotic highly correlated electronic state that can be stabilized in narrow-gap semiconductors or semimetals [1–4] via spontaneous formation of excitons below a critical temperature (T_c). Originally Bardeen-Cooper-Schieffer (BCS) theory of superconductivity was used to model the EI state [1,2] in the semimetallic regime (negative band gap E_g), where a high carrier density makes the electron-hole ($e-h$) Coulomb's attraction strongly screened for a suppressed T_c [5]. On the other hand, for semiconductors, if the exciton binding energy (E_b) exceeds E_g, a spontaneous Bose-Einstein condensation (BEC) of excitons triggers the formation of the EI state, and the coherence in bosonic wave functions leads to supertransport [4,6] and a weaker screening increases T_c [7]. The study of the EI state should give deeper insight into highly correlated phenomena like superconductivity and BEC-BCS crossover [8–10], and a plethora of theoretical and experimental investigations have been made in an effort to realize this state [7,11–14]. However, difficulty arises when trying to experimentally identify it since the excitons are neutral species whose "current" is not straightforwardly measurable. This demands investigation into other experimental signatures of the EI [7,12–14].

The realization of an EI requires highly reduced screening to Coulomb's potential that leads to a higher E_b. Low-dimensional materials tend to have reduced screening [15,16] due to confinement effect. While two-dimensional 2)D) semiconductors with a small E_g may have lower E_b because polarizability is inversely related to E_g [17], dipole forbidden transitions near the band edges are shown to break this synergy and favor the formation of an intrinsic EI state, such as in 2D GaAs [18] and graphone [19]. Another natural way of reducing screening is by increasing the $e-h$ wave function overlap [20–22], which brings electrons and holes closer, making them immune to the screening effect from surrounding charges.

The triplet EI state is especially appealing, because triplet excitons carry spin current, so that a triplet EI with spin superfluidity can be experimentally observed by spin transport measurements [23]. Triplet excitons are also attracting increasing attention in photovoltaics owing to their high radiative lifetime [24,25]. Because of the optical selection rule [26], the triplet excitons are dark but may be converted from singlets by intersystem crossing [27,28]. A large singlet-triplet splitting (ΔE_{ST}) will favor such crossing process and increase the triplet concentration at finite temperatures [29–33]. Hence, a large $e-h$ wave function overlap is especially desirable for the triplet EI formation because it increases ΔE_{ST} [30,31] by enhancing the $e-h$ exchange interaction [34].

In this Letter, we demonstrate an intriguing flat-bands-enabled mechanism that can possibly lead to the formation of triplet EI mediated by massive carriers with greatly enhanced $e-h$ wave function localization and overlap in a 2D diatomic (yin-yang) Kagome lattice [35] and further predict its realization in a real material made of superatomic graphene. Intrinsic to a topological flat band (FB) is its highly localized wave function in real space, underlined by a destructive interference of FB quantum states [36]. When a unique band-structure configuration arises, with both a topological valence and conduction FB separated by a trivial gap, it also indicates an extremely high degree of $e-h$ wave function overlap. Remarkably, the huge

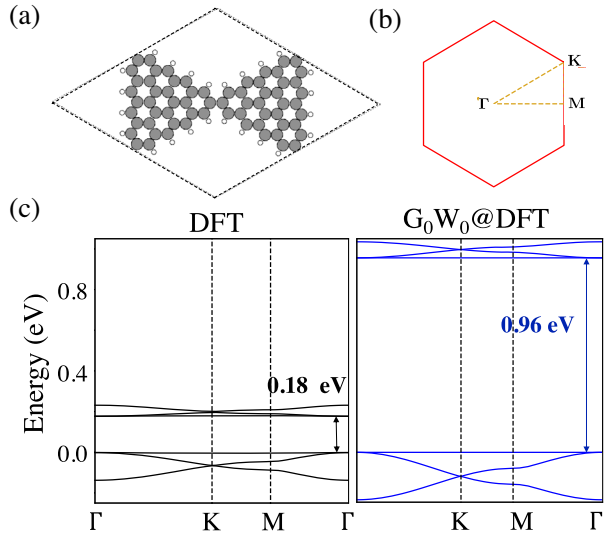

FIG. 1. (a) Unit cell of a 9×9 superatomic graphene lattice. Gray and white circles represent C and H atoms, respectively. (b) First Brillouin zone showing the high-symmetry reciprocal paths used for band diagrams. (c) Comparison of band structures and band gaps obtained within DFT (left) and a single-shot G_oW_o calculation (right).

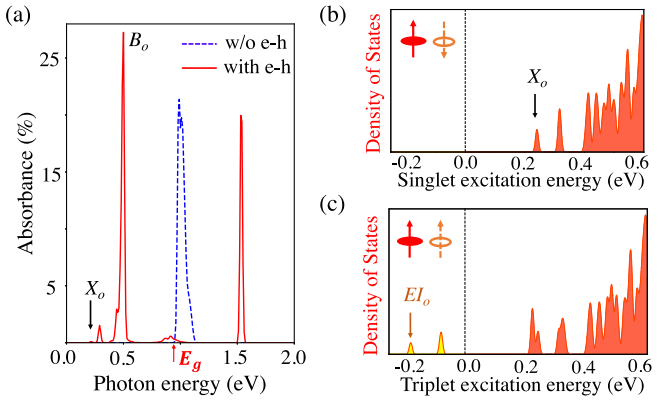

FIG. 2. (a) Optical absorbance for singlet excitons with a Gaussian peak broadening of 10 meV. X_o indicates the first bright peak. (b) Density of states for singlet excitons, and (c) density of states for triplet excitons, noticing two peaks with negative formation energies (yellow filled). EI_o indicates the first triplet exciton, which is also the case of triplet EI. Insets in (b) and (c) represent spin-up electron (red arrow with filled circle) and spin-down hole (orange arrow with hollow circle) bound together forming an exciton.

effective masses of carriers hosted in the two FBs greatly reduce the screening to increase exciton E_b, favoring the formation of EI states in general; while the highly overlapping $e-h$ wave function enhances the Coulomb's direct interaction on the one hand, to further reduce the screening, and the exchange interaction on the other hand, to increase ΔE_{ST}, favoring the formation of triplet EI states in particular. Using a superatomic graphene lattice as a prototypical example, we show the possibility of a FBs-enabled triplet EI state, based on density-functional theory (DFT) calculations combined with many-body GW and Bethe-Salpeter equation (BSE). This is indicated by a triplet exciton E_b ($\sim$1.1 eV) exceeding the GW gap ($E_g \sim 0.9$ eV) by $\sim$20% and a high ΔE_{ST} ($\sim$0.4 eV). FBs also provide an ideal platform for BEC and coherence [37] since the macroscopic degeneracy of FBs can lead to spontaneous symmetry breaking, which is central to the theory of BCS superconductivity [38,39] and EI [40,41].

Figure 1(a) shows the structure of the superatomic graphene lattice. It consists of two 9×9 graphene flakes (structural motif) with an optimized lattice constant of 22.14 Å. This peculiar structural motif enables the C atomic p_z orbitals to hybridize into molecular sp^2 orbitals, forming the so-called yin-yang Kagome bands [35] in a hexagonal lattice, as shown in Fig. 1(c). Both the highest valence and the lowest conduction bands are perfectly flat and topologically nontrivial with opposite spin Chern numbers [35]. The structure has a high thermodynamic stability with a bulk cohesive energy calculated as -6.78 eV per atom [42], similar to graphene nanoribbon [51]. Excitingly, recent experimental advances [52,53] in synthesizing nanoporous graphene suggest very high feasibility of making this lattice. These latest experiments employ a bottom-up approach to successfully make artificial nanoporous graphene lattices with precise control of pore size and shape, using designed molecular precursors. Accordingly, our theoretical study should stimulate such experimental efforts to make the proposed lattice by designing the desired superatomic graphene precursors. Also, other yin-yang Kagome lattices, such as the Kagome superlattices formed in moiré pattern twisted graphene bilayers [54], which generated a lot of recent interest, can be generally explored. Here we focus on the exciton related properties of the 9×9 superatomic graphene lattice.

First, its mean-field DFT $E_g \sim 0.18$ eV, as in a narrow-gap semiconductor, is significantly corrected to a GW $E_g \sim 0.94$ eV [Fig. 1(c)]. The optical spectra obtained by solving the BSE is shown in Fig. 2(a), in comparison with that obtained within the independent particle approximation. The first peak in the BSE spectra corresponds to the first bright singlet exciton at 0.24 eV, marked by X_o. This can also be seen from the density of states (DOS) for singlet excitons in Fig. 2(b). The formation energy of X_o is very low compared to the quasiparticle gap of 0.94 eV, giving rise to a large E_b of 0.70 eV. In Fig. 2(c), we plot the DOS for triplet excitons, which clearly shows the presence of excitons with negative formation energy, indicative of spontaneous formation of excitons. The E_b of the lowest triplet exciton ($0.94 + 0.17 = 1.11$ eV) exceeds the GW gap by 0.17 eV, to signify a desired property for a strong triplet EI state, as marked by EI_o in Fig. 2(c). This possible triplet EI in a nonmagnetic material is different from that recently studied in a ferromagnetic material, where the excitation between spin nondegenerate bands was

TABLE I. Summary of excitonic energies for states X_o and EI_o. Last column denotes the dipole oscillator strength of excitons divided by the number of k points.

Exciton	Mean-field gap (eV)	GW band gap (eV)	Excitation energy (eV)	Binding energy (eV)	Dipole oscillator strength/N_k (μ_s)
Singlet (X_o)	0.18	0.94	0.24	0.70	0.024 a.u.
Triplet (EI_o)	0.18	0.94	−0.17	1.11	⋯

considered [19]. One interesting feature is its huge ΔE_{ST} of 0.41 eV, making it easier to be detected by spin superfluidity experiment [23]. In Table I we summarize the energies of the lowest singlet (X_o) and triplet (EI_o) states. The key result of a negative triplet exciton formation energy is carefully confirmed by convergence tests for GW-BSE calculations (see Supplemental Material, Tables S1–S5 [42]).

Excitonic instability may occur in either a narrow-gap semiconductor or a semimetal [55]. In the former, a gapped system as studied here, the critical condition for the existence of the EI state is a negative exciton formation energy; i.e., if E_b exceeds E_g, the order parameter for BEC of excitons has a nontrivial solution at low temperatures. In a two-band model, the order parameter at $T = 0$ K is given by $\Delta_0 = E_b\sqrt{(\frac{1}{2}) - (E_g/2E_b)}$ [55]. As long as $E_b > E_g$, Δ_0 is finite positive and a BEC-EI state emerges below T_c. Our calculated E_b is ∼20% larger than E_g, indicating a relatively high T_c. For a system with parabolic valence and conduction bands, T_c may be estimated from a $k \cdot p$ effective-mass model [19]. However, this model is not applicable to FBs with infinite effective mass, instead, an extensive exact diagonalization approach is required to determine T_c. Differently in a semimetal, the EI state occurs below T_c' via a metal (gapless) to insulator (gapped) transition, a manifestation of spontaneous symmetry breaking [2,55]. It further involves a BCS-BEC crossover depending on the $e - h$ coupling strength [56]. One widely studied material for semimetal-to-EI transition is Ta_2NiSe_5, and a recent work [41] shows that such transition may be generally triggered by a structural transition with breaking of lattice symmetries. Also, the BEC-BCS crossover has been studied in the context of a nonequilibrium EI state [57].

In order to better understand the strikingly enhanced E_b, suggestive of the formation of triplet EI ground state below T_c, we plot the excitonic wave function in reciprocal space

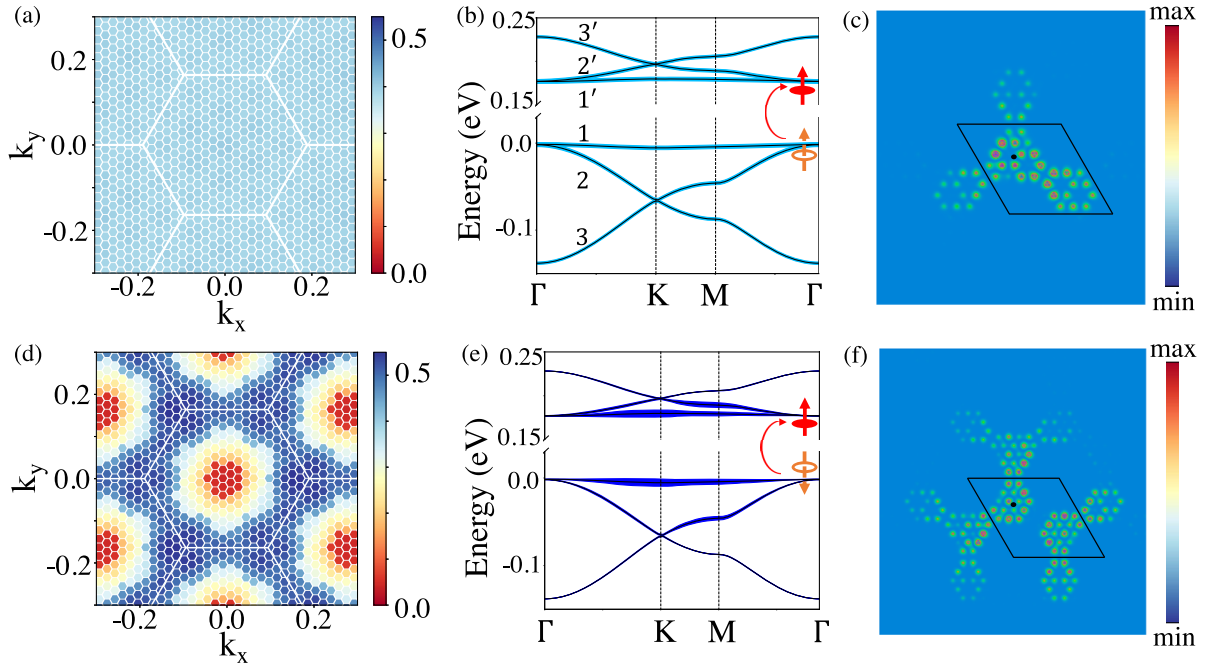

FIG. 3. Excitonic wave function analysis for the lowest triplet exciton (EI_o, upper) and for the lowest singlet exciton (X_o, lower): (a), (d) Reciprocal-space excitonic wave function distribution showing total contribution of all excitations at each reciprocal lattice point. (b),(e) Band excitation contributions indicated by spread of color on the bands. (c),(f) Real-space two-particle $e - h$ wave function distribution with hole fixed at the black dot plotted over a 6×6 supercell. Only a small segment of the supercell is shown here since the electron is highly localized around the hole. The distribution amplitude is zero everywhere else. The orange arrow with a circle denotes the spin of hole left behind after excitation and the red arrow denotes the spin of electron.

and band excitation contributions for EI_o in Figs. 3(a) and 3(b), respectively. One clearly sees that EI_o is composed of coherent excitations throughout the Brillouin zone (BZ). We also examined relative band contributions to the excitations (see Table S6 [42]). The contribution from valence to conduction FB excitation is slightly higher than from other excitations. The nature of FB excitations inherently implies localized wave functions in real space, as seen in Fig. 3(c), which shows the Fourier transform of excitonic wave function for EI_o, consistent with the broad distribution of k-point-resolved excitations (Fig. S1 [42]). This provides additional evidence for a possible BEC-EI state, because the triplet exciton width (ξ) is much smaller than the lattice constant, implying a pointlike boson, as in the BEC condensate [57–59]. In comparison, for X_o, as shown in Figs. 3(d) and 3(e), excitation from valence to conduction FB contributes the most, largely centered around the K point. The triplet EI_o state has an even more localized wave function in real space [Fig. 3(c)] than the singlet X_o [Fig. 3(f)] because the former is excited throughout the BZ; i.e., the excitonic wave function is highly delocalized in reciprocal space.

The effective static dielectric constant obtained from our calculations is unusually low ~1.02, indicating a highly reduced screening, which is a direct manifestation of FB wave functions, as we show below. Usually dipole forbidden transitions near the band edges are favored for large E_b and hence the formation of the EI state [17–19]. For the yin-yang FBs, the inter-FB transitions are actually allowed by symmetry [35] but the band flatness makes the dipole matrix element between them negligible. Considering a two-band model, the dipole matrix element is given by

$$|\langle u_{c,k}|\nabla_k|u_{v,k}\rangle|^2 = \frac{\hbar^2}{2\mu}\left(E_g + \frac{\hbar^2 k^2}{2\mu}\right)^{-1}, \qquad (1)$$

where μ is the reduced mass under the effective-mass approximation [17], which is very high here for both valence and conduction FBs, making the above expression close to zero. A negligible dipole matrix element is directly verified from the absence of absorption peak at E_g in the optical spectrum [Fig. 2(a)] obtained within the independent particle approximation (see also Fig. S4 [42]). This also explains the very low absorbance for X_o [Fig. 2(a)], since the major contribution to this state is from FB excitations, and its nonzero portion of absorption is mostly contributed by weaker transitions that involve parabolic bands (e.g., $1 \rightarrow 2'$ near M point) as shown in Fig. 3(e). Basically, only parabolic-band transitions lead to high optical absorption. The detailed contributions from individual band excitations are available in the Supplemental Material [42] (Table S1 and Fig. S2), and the band-resolved contributions to the brightest exciton, marked in Fig. 2(a) by B_o, is available in Fig. S3 [42]. Since 2D polarizability is proportional to the dipole matrix element divided by the gap [17], the presence of FBs as both the highest occupied valence and the lowest unoccupied conduction bands inherently reduces the screening significantly.

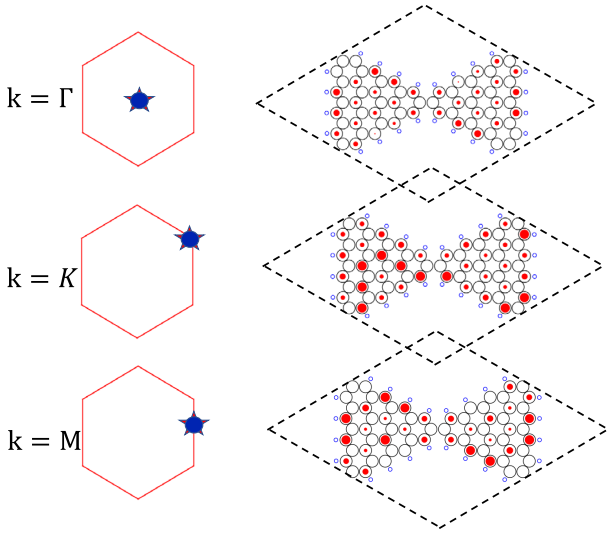

FIG. 4. Conduction and valence FBs wave function overlap for zero momentum singlet exciton ($Q = 0$). Right: C and H atoms are indicated by large and small circles, respectively. The contributions are only from the C p_z orbitals. The overlapped weights of these contributions to flat valence and conduction band wave functions are indicated by the size of red fills on the C atoms. Left: k points in BZ for which overlaps are calculated.

Normally, reduced screening and confinement effects in low dimensions are known to extrinsically increase the $e-h$ wave function overlap as shown in heteronanostructures [29] and carbon nanotubes [30]. Interestingly, here both electron and hole wave functions exhibit a form of destructive quantum interference originated from the FB topology [36], which gives rise to their distinguished localized states in real space with huge overlap. Figure 4 shows the relative overlap between the two FB wave functions at high-symmetry k points projected over atomic orbitals of C and H. Such huge overlap leads to a much higher energy for singlet compared to triplet excitons, as the exchange interaction is absent in the latter. This represents a unique *intrinsic* FB originated increase of direct and exchange energy, leading to a ΔE_{ST} of ~0.4 eV, much larger than the typical values in bulk (a few meVs) [29] and low-dimensional semiconductors (up to ~0.2 eV) [30–33]. Thus, both a huge $e-h$ wave function overlap and a highly reduced screening, as induced by the FBs, are the major factors leading to a large E_b, and an enhanced ΔE_{ST}, favorable for a triplet EI. More singlet exciton properties are given in the Supplemental Material [42].

For comparison, it might be interesting to construct a supermolecule consisting of two superatomic graphene flakes and study its excitonic properties, for which a Frenkel type of localized exciton is expected. Also, in

the condensed state of van der Waals molecular crystals, excitons with relatively large E_b and almost linear excitonic dispersion have been previously shown [60]. In contrast, for the covalently bonded framework we study here, the highly localized and overlapping exciton wave functions, as shown in Figs. 3(c) and 3(f), are enabled by FBs, having a very different physical origin. This is because the FB is a Bloch state; it is encoded with nontrivial topology, arising from destructive interference of lattice hopping that leads to compact plaquette states of both electrons and holes in real space [35]. As such, the excitons display an unusual constant dispersion (see also the discussion for singlet excitons in the Supplemental Material [42]).

In conclusion, we reveal a unique topological FB-originated mechanism for the possible formation of a spin triplet EI, making a significant forward step for the discovery of EIs through spin transport measurement. In a 9×9 superatomic graphene lattice, a triplet exciton E_b is predicted to exceed the band gap by $\sim$0.2 eV. The FBs, generally existing in a yin-yang Kagome lattice, weaken intrinsically the screened $e - h$ interaction by an "infinite" effective mass of carriers and a complete overlap of $e - h$ wave functions, and the latter also increases the exchange energy of singlet exciton leading to a huge ΔE_{ST}. In general, defects are likely present in experimental samples. However, if the defect density is kept low, there is usually no significant change in the screening and excitonic properties, as shown in transition metal dichalcogenides [61]. Spin-orbit coupling (SOC) may have interesting consequences in our proposal; however, since only C and H atoms are present here, it is negligible and not considered. Other yin-yang Kagome lattice materials with large SOC are interesting topics for future studies, especially in considering the related phenomena of excited quantum anomalous and spin Hall effect [35]. Furthermore, fractional population of two FBs may lead to an exotic fractional EI state [62].

G. S, Y. Z., and F. L. acknowledge financial support from U.S. Department of Energy–Basic Energy Sciences (Award No. DE-FG02- 04ER46148). L. Z. and L. Y. are supported by the Air Force Office of Scientific Research (AFOSR) Grant No. FA9550-20-1-0255 and the National Science Foundation (NSF) CAREER Grant No. DMR-1455346. The calculations were done on the CHPC at the University of Utah and DOE-NERSC.

[1] W. Kohn, Excitonic Phases, Phys. Rev. Lett. **19**, 439 (1967).
[2] D. Jérome, T. Rice, and W. Kohn, Excitonic insulator, Phys. Rev. **158**, 462 (1967).
[3] N. F. Mott, The transition to the metallic state, Philos. Mag. **6**, 287 (1961).
[4] B. Halperin and T. Rice, Possible anomalies at a semimetal-semiconductor transition, Rev. Mod. Phys. **40**, 755 (1968).
[5] F. X. Bronold and H. Fehske, Possibility of an excitonic insulator at the semiconductor-semimetal transition, Phys. Rev. B **74**, 165107 (2006).
[6] W. Kohn and D. Sherrington, Two kinds of bosons and Bose condensates, Rev. Mod. Phys. **42**, 1 (1970).
[7] Y. Lu, H. Kono, T. Larkin, A. Rost, T. Takayama, A. Boris, B. Keimer, and H. Takagi, Zero-gap semiconductor to excitonic insulator transition in Ta_2NiSe_5, Nat. Commun. **8**, 14408 (2017).
[8] V.-N. Phan, K. W. Becker, and H. Fehske, Spectral signatures of the BCS-BEC crossover in the excitonic insulator phase of the extended Falicov-Kimball model, Phys. Rev. B **81**, 205117 (2010).
[9] B. Zenker, D. Ihle, F. Bronold, and H. Fehske, Electron-hole pair condensation at the semimetal-semiconductor transition: A BCS-BEC crossover scenario, Phys. Rev. B **85**, 121102(R) (2012).
[10] K. Seki, Y. Wakisaka, T. Kaneko, T. Toriyama, T. Konishi, T. Sudayama, N. Saini, M. Arita, H. Namatame, M. Taniguchi, N. Katayama, M. Nohara, H. Takagi, T. Mizokawa, and Y. Ohta, Excitonic Bose-Einstein condensation in Ta_2NiSe_5 above room temperature, Phys. Rev. B **90**, 155116 (2014).
[11] B. Bucher, P. Steiner, and P. Wachter, Excitonic Insulator Phase in $TmSe_{0.45}Te_{0.55}$, Phys. Rev. Lett. **67**, 2717 (1991).
[12] Y. Wakisaka, T. Sudayama, K. Takubo, T. Mizokawa, M. Arita, H. Namatame, M. Taniguchi, N. Katayama, M. Nohara, and H. Takagi, Excitonic Insulator State in Ta_2NiSe_5 Probed by Photoemission Spectroscopy, Phys. Rev. Lett. **103**, 026402 (2009).
[13] L. Du, X. Li, W. Lou, G. Sullivan, K. Chang, J. Kono, and R.-R. Du, Evidence for a topological excitonic insulator in InAs/GaSb bilayers, Nat. Commun. **8**, 1971 (2017).
[14] Z. Li, M. Nadeem, Z. Yue, D. Cortie, M. Fuhrer, and X. Wang, Possible excitonic insulating phase in quantum-confined Sb nanoflakes, Nano Lett. **19**, 4960 (2019).
[15] A. Chernikov, T. C. Berkelbach, H. M. Hill, A. Rigosi, Y. Li, O. B. Aslan, D. R. Reichman, M. S. Hybertsen, and T. F. Heinz, Exciton Binding Energy and Nonhydrogenic Rydberg Series in Monolayer Ws_2, Phys. Rev. Lett. **113**, 076802 (2014).
[16] P. Cudazzo, L. Sponza, C. Giorgetti, L. Reining, F. Sottile, and M. Gatti, Exciton Band Structure in Two-Dimensional Materials, Phys. Rev. Lett. **116**, 066803 (2016).
[17] Z. Jiang, Z. Liu, Y. Li, and W. Duan, Scaling Universality between Band Gap and Exciton Binding Energy of Two-Dimensional Semiconductors, Phys. Rev. Lett. **118**, 266401 (2017).
[18] Z. Jiang, Y. Li, S. Zhang, and W. Duan, Realizing an intrinsic excitonic insulator by decoupling exciton binding energy from the minimum band gap, Phys. Rev. B **98**, 081408(R) (2018).
[19] Z. Jiang, W. Lou, Y. Liu, Y. Li, H. Song, K. Chang, W. Duan, and S. Zhang, Spin-Triplet Excitonic Insulator: The Case of Semihydrogenated Graphene, Phys. Rev. Lett. **124**, 166401 (2020).
[20] J.-C. Blancon, A. V. Stier, H. Tsai, W. Nie, C. C. Stoumpos, B. Traore, L. Pedesseau, M. Kepenekian, F. Katsutani, G. Noe *et al.*, Scaling law for excitons in 2D perovskite quantum wells, Nat. Commun. **9**, 2254 (2018).

[21] W. Wei, Y. Dai, B. Huang, and T. Jacob, Enhanced many-body effects in 2- and 1-dimensional ZNO structures: A Green's function perturbation theory study, J. Chem. Phys. **139**, 144703 (2013).

[22] M. Goryca, J. Li, A. V. Stier, T. Taniguchi, K. Watanabe, E. Courtade, S. Shree, C. Robert, B. Urbaszek, X. Marie *et al.*, Revealing exciton masses and dielectric properties of monolayer semiconductors with high magnetic fields, Nat. Commun. **10**, 4172 (2019).

[23] Q.-F. Sun, Z.-T. Jiang, Y. Yu, and X. C. Xie, Spin superconductor in ferromagnetic graphene, Phys. Rev. B **84**, 214501 (2011).

[24] B. T. Luppi, D. Majak, M. Gupta, E. Rivard, and K. Shankar, Triplet excitons: Improving exciton diffusion length for enhanced organic photovoltaics, J. Mater. Chem. A **7**, 2445 (2019).

[25] M. Einzinger, T. Wu, J. F. Kompalla, H. L. Smith, C. F. Perkinson, L. Nienhaus, S. Wieghold, D. N. Congreve, A. Kahn, M. G. Bawendi *et al.*, Sensitization of silicon by singlet exciton fission in tetracene, Nature (London) **571**, 90 (2019).

[26] T. Mueller and E. Malic, Exciton physics and device application of two-dimensional transition metal dichalcogenide semiconductors, npj 2D Mater. Appl. **2**, 29 (2018).

[27] J. Palotás, M. Negyedi, S. Kollarics, A. Bojtor, P. Rohringer, T. Pichler, and F. Simon, Incidence of quantum confinement on dark triplet excitons in carbon nanotubes, ACS Nano **14**, 11254 (2020).

[28] M. Kasha, Characterization of electronic transitions in complex molecules, Discuss. Faraday Soc. **9**, 14 (1950).

[29] H. Fu, L.-W. Wang, and A. Zunger, Excitonic exchange splitting in bulk semiconductors, Phys. Rev. B **59**, 5568 (1999).

[30] A. Granados Del Águila, E. Groeneveld, J. C. Maan, C. de Mello Donegá, and P. C. Christianen, Effect of electron-hole overlap and exchange interaction on exciton radiative lifetimes of CdTe/CdSe heteronanocrystals, ACS Nano **10**, 4102 (2016).

[31] V. Perebeinos, J. Tersoff, and P. Avouris, Radiative lifetime of excitons in carbon nanotubes, Nano Lett. **5**, 2495 (2005).

[32] M. Nirmal, D. J. Norris, M. Kuno, M. G. Bawendi, A. L. Efros, and M. Rosen, Observation of the"Dark Exciton" in CdSe Quantum Dots, Phys. Rev. Lett. **75**, 3728 (1995).

[33] D. J. Norris, A. L. Efros, M. Rosen, and M. G. Bawendi, Size dependence of exciton fine structure in CdSe quantum dots, Phys. Rev. B **53**, 16347 (1996).

[34] M. Rohlfing and S. G. Louie, Electron-hole excitations and optical spectra from first principles, Phys. Rev. B **62**, 4927 (2000).

[35] Y. Zhou, G. Sethi, H. Liu, Z. Wang, and F. Liu, Excited quantum Hall effect: Enantiomorphic flat bands in a yin-yang Kagome lattice, arXiv:1908.03689.

[36] L. Zheng, L. Feng, and W. Yong-Shi, Exotic electronic states in the world of flat bands: From theory to material, Chin. Phys. B **23**, 077308 (2014).

[37] S. D. Huber and E. Altman, Bose condensation in flat bands, Phys. Rev. B **82**, 184502 (2010).

[38] S. Weinberg, *The Quantum Theory of Fields* (Cambridge University Press, Cambridge, 1995), Vol. 2.

[39] S. Weinberg, Superconductivity for particular theorists, Prog. Theor Phys. Suppl. **86**, 43 (1986).

[40] T. Kaneko, K. Seki, and Y. Ohta, Excitonic insulator state in the two-orbital Hubbard model: Variational cluster approach, Phys. Rev. B **85**, 165135 (2012).

[41] G. Mazza, M. Rösner, L. Windgätter, S. Latini, H. Hübener, A. J. Millis, A. Rubio, and A. Georges, Nature of Symmetry Breaking at the Excitonic Insulator Transition: Ta_2NiSe_5, Phys. Rev. Lett. **124**, 197601 (2020).

[42] See Supplemental Material at http://link.aps.org/supplemental/10.1103/PhysRevLett.126.196403 for computational details, convergence study of GW-BSE, and additional discussion on the material stability, excitonic wavefunction distributions, negligible absorption between the flat bands, e-h pair correlation function and lifetime of singlet excitons, which includes Refs. [43–50].

[43] J. P. Perdew, K. Burke, and M. Ernzerhof, Generalized Gradient Approximation made Simple, Phys. Rev. Lett. **77**, 3865 (1996).

[44] P. Giannozzi, S. Baroni, N. Bonini, M. Calandra, R. Car, C. Cavazzoni, D. Ceresoli, G. L. Chiarotti, M. Cococcioni, I. Dabo *et al.*, QUANTUM ESPRESSO: A modular and open-source software project for quantum simulations of materials, J. Phys. Condens. Matter **21**, 395502 (2009).

[45] J. Deslippe, G. Samsonidze, D. A. Strubbe, M. Jain, M. L. Cohen, and S. G. Louie, BERKELEYGW: A massively parallel computer package for the calculation of the quasiparticle and optical properties of materials and nanostructures, Comput. Phys. Commun. **183**, 1269 (2012).

[46] M. S. Hybertsen and S. G. Louie, Electron correlation in semiconductors and insulators: Band gaps and quasiparticle energies, Phys. Rev. B **34**, 5390 (1986).

[47] V. Barone, O. Hod, and G. E. Scuseria, Electronic structure and stability of semiconducting graphene nanoribbons, Nano Lett. **6**, 2748 (2006).

[48] R. Gillen and J. Maultzsch, Light-matter interactions in two-dimensional transition metal dichalcogenides: Dominant excitonic transitions in mono-and few-layer MoX_2 and band nesting, IEEE J. Sel. Top. Quantum Electron. **23**, 219 (2016).

[49] M. Palummo, M. Bernardi, and J. C. Grossman, Exciton radiative lifetimes in two-dimensional transition metal dichalcogenides, Nano Lett. **15**, 2794 (2015).

[50] C. D. Spataru, S. Ismail-Beigi, R. B. Capaz, and S. G. Louie, Theory and Ab Initio Calculation of Radiative Lifetime of Excitons in Semiconducting Carbon Nanotubes, Phys. Rev. Lett. **95**, 247402 (2005).

[51] V. Barone, O. Hod, and G. E. Scuseria, Electronic structure and stability of semiconducting graphene nanoribbons, Nano Lett. **6**, 2748 (2006).

[52] P. H. Jacobse, R. D. McCurdy, J. Jiang, D. J. Rizzo, G. Veber, P. Butler, R. Zuzak, S. G. Louie, F. R. Fischer, and M. F. Crommie, Bottom-up assembly of nanoporous graphene with emergent electronic states, J. Am. Chem. Soc. **142**, 13507 (2020).

[53] C. Moreno, M. Vilas-Varela, B. Kretz, A. Garcia-Lekue, M. V. Costache, M. Paradinas, M. Panighel, G. Ceballos, S. O. Valenzuela, D. Peña *et al.*, Bottom-up synthesis of multifunctional nanoporous graphene, Science **360**, 199 (2018).

[54] A. Ramires and J. L. Lado, Electrically Tunable Gauge Fields in Tiny-Angle Twisted Bilayer Graphene, Phys. Rev. Lett. **121**, 146801 (2018).

[55] A. Kozlov and L. Maksimov, The metal-dielectric divalent crystal phase transition, Sov. Phys. JETP **2**, 790 (1965).
[56] K. Sugimoto, S. Nishimoto, T. Kaneko, and Y. Ohta, Strong Coupling Nature of the Excitonic Insulator State in Ta_2NiSe_5, Phys. Rev. Lett. **120**, 247602 (2018).
[57] E. Perfetto, D. Sangalli, A. Marini, and G. Stefanucci, Pump-driven normal-to-excitonic insulator transition: Josephson oscillations and signatures of BEC-BCS crossover in time-resolved ARPES, Phys. Rev. Materials **3**, 124601 (2019).
[58] T. Kaneko, S. Ejima, H. Fehske, and Y. Ohta, Exact-diagonalization study of exciton condensation in electron bilayers, Phys. Rev. B **88**, 035312 (2013).
[59] T. Kaneko, Theoretical study of excitonic phases in strongly correlated electron systems, Ph.D. thesis, Department of Physics, Chiba University (2016).
[60] P. Cudazzo, F. Sottile, A. Rubio, and M. Gatti, Exciton dispersion in molecular solids, J. Phys. Condens. Matter **27**, 113204 (2015).
[61] S. Refaely-Abramson, D. Y. Qiu, S. G. Louie, and J. B. Neaton, Defect-Induced Modification of Low-Lying Excitons and Valley Selectivity in Monolayer Transition Metal Dichalcogenides, Phys. Rev. Lett. **121**, 167402 (2018).
[62] Y. Hu, J. W. F. Venderbos, and C. L. Kane, Fractional Excitonic Insulator, Phys. Rev. Lett. **121**, 126601 (2018).